Geophys. J. Int. (2007) **169,** 1069–1078 doi: 10.1111/j.1365-246X.2006.03262.x

Frequency response modelling of seismic waves using finite difference time domain with phase sensitive detection (TD–PSD)

Kurt T. Nihei[1] and Xiaoye Li[2]

[1]*Earth Sciences Division, Lawrence Berkeley National Laboratory; now at Chevron ETC,* 6001 *Bollinger Canyon Rd., San Ramon,* CA 94583, *USA. E-mail: knih@chevron.com*
[2]*Computational Research Division, Lawrence Berkeley National Laboratory,* 1 *Cyclotron Rd.,* MS 50F-1650, *Berkeley,* CA 94720, *USA*

Accepted 2006 October 11. Received 2006 October 11; in original form 2005 August 26

SUMMARY

This paper describes an efficient approach for computing the frequency response of seismic waves propagating in 2- and 3-D earth models within which the magnitude and phase are required at many locations. The approach consists of running an explicit finite difference time domain (TD) code with a time harmonic source out to steady-state. The magnitudes and phases at locations in the model are computed using phase sensitive detection (PSD). PSD does not require storage of time-series (unlike a fast Fourier transform), reducing its memory requirements. Additionally, the response from multiple sources can be obtained from a single finite difference run by encoding each source with a different frequency. For 2-D models with many sources, this time domain phase sensitive detection (TD–PSD) approach has a higher arithmetic complexity than direct solution of the finite difference frequency domain (FD) equations using nested dissection re-ordering (FD–ND). The storage requirements for 2-D finite difference TD–PSD are lower than FD–ND. For 3-D finite difference models, TD–PSD has significantly lower arithmetic complexity and storage requirements than FD–ND, and therefore, may prove useful for computing the frequency response of large 3-D earth models.

Key words: finite-difference methods, numerical techniques, seismic modelling.

1 INTRODUCTION

Computation of the frequency response (phase and magnitude) of seismic waves propagating in heterogeneous, anisotropic, viscoelastic media is required for a number of scientific and engineering endeavors, including frequency domain full-waveform inversion, earthquake site response modelling and structural vibration studies. When the frequency response is required at a limited number of locations, it can be computed efficiently with a finite difference time domain (TD) code by storing the time-series at specified receiver locations and computing the magnitude and phase with a fast Fourier transform (FFT). However, when the frequency response is required at many or all grid locations in the model, as in frequency domain (FD) full-waveform inversion (e.g. Pratt *et al.* 1998), the memory requirements for storing the waveforms at many model locations (for subsequent FFT analysis) make this approach prohibitive.

An alternative approach is to compute the frequency response by reformulating the finite difference equations in the FD (Marfurt 1984; Štekl & Pratt 1998; Hustedt *et al.* 2004). The resulting linear system has the form $\boldsymbol{Ku} = \boldsymbol{f}$. For fourth-order accuracy spatial differencing on a 2-D elastic $n \times n$ finite difference staggered grid, the system of implicit equations for $\boldsymbol{u}$ (the unknown particle velocities and stresses) at the finite difference cell locations is a large, complex, banded (band-diagonal with eight subbands), sparse, non-Hermitian system matrix $\boldsymbol{K}$ with $O(n^2)$ non-zero entries. Direct solution of the 2-D matrix using LU-factorization with nested dissection (ND) re-ordering requires $O(n^2 \log_2 n)$ storage and $O(n^3)$ operations (arithmetic complexity), and, for an $n \times n \times n$ 3-D problem, $O(n^4)$ storage and $O(n^6)$ operations (George & Liu 1981). An attractive feature of direct solution is its ability to provide solutions for additional sources $\boldsymbol{f}$ via a low cost backsubstitution. For typical 2-D seismic exploration models [e.g. 10 000 × 2500, $\boldsymbol{K}$ of $O(10^8)$] with several hundred sources, high performance sparse direct solution of the frequency domain system via nested dissection (FD–ND) (Li & Demmel 2003) is an efficient approach for computing of the entire-model frequency response. For large 3-D problems, however, direct solution requires a prohibitive $O(n^6)$ operations. A viable alterative is to solve $\boldsymbol{Ku} = \boldsymbol{f}$ with an iterative method, recognizing that a separate iterative solution is now required for each source. For 3-D problems, a simple Krylov iterative solver without preconditioning and blocking requires $O(n^3)$ storage and a sparse matrix–vector multiplication requiring $O(n^3)$ operations per iteration. To speed up convergence, Krylov methods require a preconditioner (Barrett *et al.* 1994). For 2-D acoustic wave propagation, Plessix & Mulder (2003) show that a separation-of-variables preconditioner and a bi-conjugate gradient (BICGSTAB) Krylov iterative solver yield acceptable convergence for smooth models and low frequencies. Unfortunately, poor convergence was observed as the frequency of the wave and the roughness of the model increase to values typically encountered in seismic exploration problems.

In the following sections, we examine an alternative approach for computing the frequency response of a heterogeneous, anisotropic, viscoelastic medium. The approach consists of running an explicit finite difference TD code with a harmonic wave source out to steady-state, and then extracting the magnitude and phase from the transient data via phase sensitive detection (PSD). The PSD algorithm requires integration over a single cycle of the waveform to obtain accurate phase and magnitude estimates. Because this integration is performed by a summation over time, it is not necessary to store waveforms at all the grid locations, as would be required if a FFT was employed. We also demonstrate that the response of multiple sources at different spatial locations can be obtained in a single finite difference run by encoding each source with a different frequency and extracting the phase and magnitude fields for each source (i.e. each frequency) via the PSD algorithm.

2 ENTIRE-MODEL FREQUENCY RESPONSE MODELLING WITH FINITE DIFFERENCE TIME DOMAIN AND PHASE SENSITIVE DETECTION (TD–PSD)

In principle, the phase and magnitude fields can be computed from a finite difference TD code by recording the time-series at all locations in the model that are generated by a broad-band source. For a 2-D $n \times n$ model, this approach requires storage of n^2 time-series of length N i.e. $O(n^2 N)$ storage and n^2 FFT i.e. $O(n^2 N \log_2 N)$ operations; (i.e. Press *et al.* 1992). For a 3-D $n \times n \times n$ model, this approach requires $O(n^3 N)$ storage and $O(n^3 N \log_2 N)$ operations. The large storage requirements make this approach intractable for large 2-D and modest size 3-D models.

2.1 Phase sensitive detection (PSD)

Here, we describe an alternative approach that can recover the magnitude and phase fields at a single frequency from finite difference TD simulations performed with a time harmonic source. The approach, which is commonly employed in digital lock-in amplifiers to recover the magnitude and phase of very small AC signals with exceptionally high accuracy (e.g. Stanford Research Systems 1999), is referred to as PSD. The PSD algorithm uses a reference waveform and a 90° phase shifted version of this reference waveform to compute the magnitude $E_{\rm sig}$ and phase $\theta_{\rm sig}$ of the recorded signal $\varepsilon_{\rm sig}$

$$\begin{aligned}
\varepsilon_{\rm sig} &= E_{\rm sig}\cos(\omega t + \theta_{\rm sig}) \quad \text{signal,}\\
\varepsilon_{\rm ref0^\circ} &= E_{\rm ref}\cos(\omega t + \theta_{\rm ref}) \quad \text{reference (in-phase),}\\
\varepsilon_{\rm ref90^\circ} &= E_{\rm ref}\cos(\omega t + \theta_{\rm ref} + 90^\circ) \quad \text{reference (out-of-phase).} \qquad (1)
\end{aligned}$$

The cross-correlation of the recorded signal $\varepsilon_{\rm sig}$ with the reference $\varepsilon_{\rm ref0^\circ}$ over an integer number of periods mT gives the in-phase component of the signal X

$$X = \frac{1}{mT}\int_{t_S}^{t_S+mT} [\varepsilon_{\rm sig}\cdot\varepsilon_{\rm ref0^\circ}]\, dt. \qquad (2)$$

The cross-correlation of the recorded signal $\varepsilon_{\rm sig}$ with the 90° phase shifted reference $\varepsilon_{\rm ref90^\circ}$ over an integer number of periods mT gives the out-of-phase component of the signal Y

$$Y = \frac{1}{mT}\int_{t_S}^{t_S+mT} [\varepsilon_{\rm sig}\cdot\varepsilon_{\rm ref90^\circ}]\, dt\,. \qquad (3)$$

The magnitude and phase of the signal are computed from the in-phase and out-of-phase components

$$\begin{aligned}
E_{\rm sig} &= 2\sqrt{X^2+Y^2}/E_{\rm ref}\\
\theta_{\rm sig} &= \tan^{-1}(Y/X) + \theta_{\rm ref}, \qquad (4)
\end{aligned}$$

which can be verified by substitution of eqs (1)–(3) into eq. (4).

Practical implementation of the PSD approach in a finite difference TD code requires two pieces of information: (1) a starting time t_S at which the integration should commence, and (2) the number of periods mT required for an accurate estimate of the magnitude and phase. For the former, a simple criterion based on the traveltime of the slowest shear waves in the model is used (Appendix A). For the latter, experience with the TD–PSD approach has demonstrated that a single period (i.e. $m = 1$) of integration is sufficient to obtain accurate phase and magnitude estimates.

Because the PSD approach requires a simple integration over time, the magnitude and phase computations do not require the storage of time-series. This significantly reduces the storage requirements over the FFT approach in applications that require the computation of the magnitude and phase at many locations in the finite difference model, such as FD full-waveform inversion (Pratt *et al.* 1998; Sirgue & Pratt 2004). It should be noted that, taken collectively, the PSD eqs (1)–(3) have the form of a discrete Fourier transform (DFT) for the specific case where the signal is a harmonic wave, the reference wave has a magnitude of 1 and a phase of zero (i.e. $E_{\rm ref} = 1$ and $\theta_{\rm ref} = 0$), and the integration is over integer multiples of the wave period T. The application of a DFT, which like PSD, is also a running sum over time calculation, to extract the frequency response of finite difference TD electromagnetic wave propagation simulations is described by Furse (2000).

2.2 Accuracy test

The accuracy of the TD–PSD approach for computing the phase and magnitude fields is established for a 2-D isotropic elastic inclusion model through a comparison with a FD boundary element method (BEM) solution (Nihei 2005). Because the BEM solution is constructed from the analytic Green's function for elastic waves, experience has shown that it can be very accurate when the numerical integration is performed at ∼8–10 points per shear wavelength. However, the computational expense of forming and solving the implicit system of complex, non-sparse BEM equations limits its applicability to simplistic earth models.

For the BEM-finite difference TD–PSD comparison, the model consists of a square region containing higher P- and S-wave velocities (Fig. 1). A vertical body force source driven at 30 Hz excites both P and S waves that superimpose in space and time to form simple harmonic particle motion at every point in the model (Fig. 1).

The finite difference TD modelling was carried out using an elastic staggered grid code with $O(2)$ time and $O(4)$ space differencing accuracies (Levander 1988). The magnitude and phase fields are computed via the PSD approach (i.e. eqs 1–4). The integrations in eqs (2) and (3) are started at $t_S = 0.4$ s. A comparison of the recorded particle velocity at a location $x = 200$ m, $z = -600$ m and that reconstructed from the PSD computed magnitudes and phases is displayed in Fig. 2. At this particular receiver location, simple harmonic motion (i.e. a steady-state) is achieved by 0.4 s. Accurate PSD estimates of the particle velocity are evident at integer multiples of the wave period $T = 1/(30\ \text{Hz})$, where the cross-correlations in eqs (2) and (3) ‘ lock-in ’ to the correct magnitude and phase.

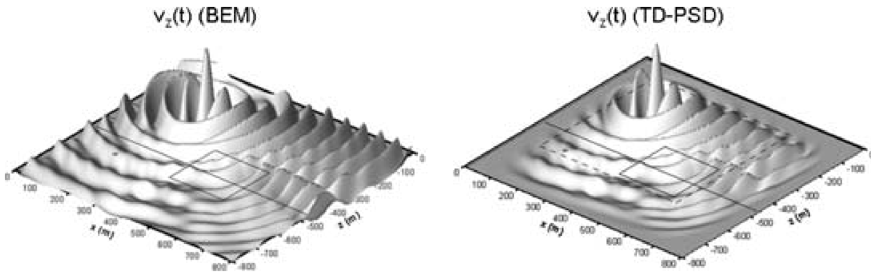

Figure 1. Snapshots of the vertical particle velocity taken at $\omega t = \pi$: (left) BEM, and (right) reconstructed from the finite difference TD–PSD computed magnitudes and phases. The model consists of a higher velocity 200×200 m square inclusion ($V_P = 4000$ m s^{-1}, $V_S = 2406$ m s^{-1}, $\rho = 2200$ kg m^{-3}) embedded in an infinite space ($V_P = 3300$ m s^{-1}, $V_S = 1700$ m s^{-1}, $\rho = 2350$ kg m^{-3}). The source is a vertical body force driven at 30 Hz. The results show very close agreement except in the outer 150 m of the finite difference TD model (region outside the dashed lines) where absorbing boundaries are applied.

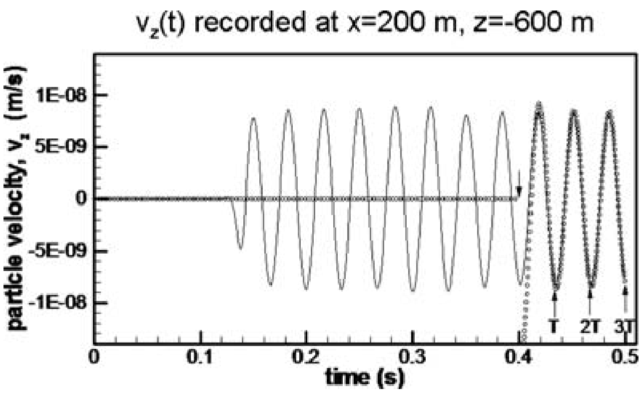

Figure 2. Finite difference TD particle velocity (vertical component) at a location $x = 200$ m, $z = -600$ m: (solid) recorded, and (dotted) reconstructed from the TD–PSD computed magnitude and phase. The arrows indicate integral multiples of the wave period T where the PSD integration 'locks-in' to the correct particle velocity magnitude and phase.

A comparison of the BEM and finite difference TD–PSD computed magnitudes is shown in Fig. 3 for the vertical particle velocity. The finite difference TD–PSD computed magnitude and phase fields show very good agreement in the region interior to the absorbing boundaries (indicated by the dashed box).

Detailed comparisons of the magnitude and phase fields along the profile at $z = -500$ m are displayed in Fig. 4. The agreement between the BEM and finite difference TD–PSD magnitudes and phases is very good in the region interior to the absorbing boundaries of the finite difference model.

2.3 SEG/EAGE salt model example

The subsurface can exhibit a range of complexities for elastic waves, including multiscale heterogeneities, anisotropy and attenuation. To be of practical value, the TD–PSD approach must be capable of computing the frequency response in earth models with realistic complexity. In this section, TD–PSD is used to extract the frequency response of elastic waves propagating in the 2-D SEG/EAGE salt model (Aminzadeh *et al.* 1994).

The 2-D SEG/EAGE salt model contains a high velocity salt body embedded in faulted and variable thickness sediments typical of the Gulf of Mexico (Fig. 5). The model is isotropic with a constant density (2450 kg m^{-3}) and a constant Poisson's ratio ($\nu = 0.25$). The 16.2×3.7 km finite difference model was discretized into 12.2×12.2 m cells to form a 1324×300 mesh. A stress-free boundary condition was set at the top of the model to represent the surface of the ocean. A 30 Hz cosine wave (tapered on its leading edge) was injected 3.7 m below the ocean surface at location $x = 3.7$ km. The finite difference simulations on this model were carried out to 41 s with a time step of 1.5 ms using an O(2,4) viscoelastic staggered grid finite difference TD code (Robertsson *et al.* 1994).

Traces for a receiver located in the bottom right-hand corner of the model ($x = 15.1$ km, $z = 3.1$ km) are displayed in Fig. 6 for two values of attenuation: $Q = \infty$ (zero attenuation) and $Q = 150$ (considered near the upper bound of Q values for Gulf of Mexico sediments). This result demonstrates the long times required to achieve steady-state (i.e. simple harmonic motion) in a purely elastic model. In fact, the traces in Fig. 6 show that a steady-state condition is not achieved in the 41 s simulation time for the $Q = \infty$ model, while it is achieved at $\sim$15 s in the $Q = 150$ model. Thus, incorporating realistic Q values in the model can significantly reduce the number of time steps required to achieve steady-state conditions.

The magnitude and phase of the vertical particle velocity were computed at every cell in the finite difference model, and are displayed in Fig. 7 for the two Q values. As expected, attenuation has a strong effect on the spatial decay of the magnitude away from the source, while the corresponding phase changes are more subtle.

3 MULTISOURCE MODELLING USING TD–PSD WITH FREQUENCY-ENCODED SOURCES

Frequency response measurements by a lock-in detector are made possible by the PSD ' s ability to accurately isolate the frequency response at the specified frequency while rejecting contributions from other frequencies (Stanford Research Systems 1999). This feature can be exploited in finite difference TD–PSD modelling to compute the frequency response at multiple frequencies from a single run by superimposing multiple frequencies at the source or to compute the frequency response for multiple sources by encoding each with a slightly different frequency. Multifrequency PSD is described in further detail below.

3.1 Multifrequency PSD

When multiple frequencies are present in the signal, beating (modulation) will occur (Kinsler *et al.* 1982), thereby altering the

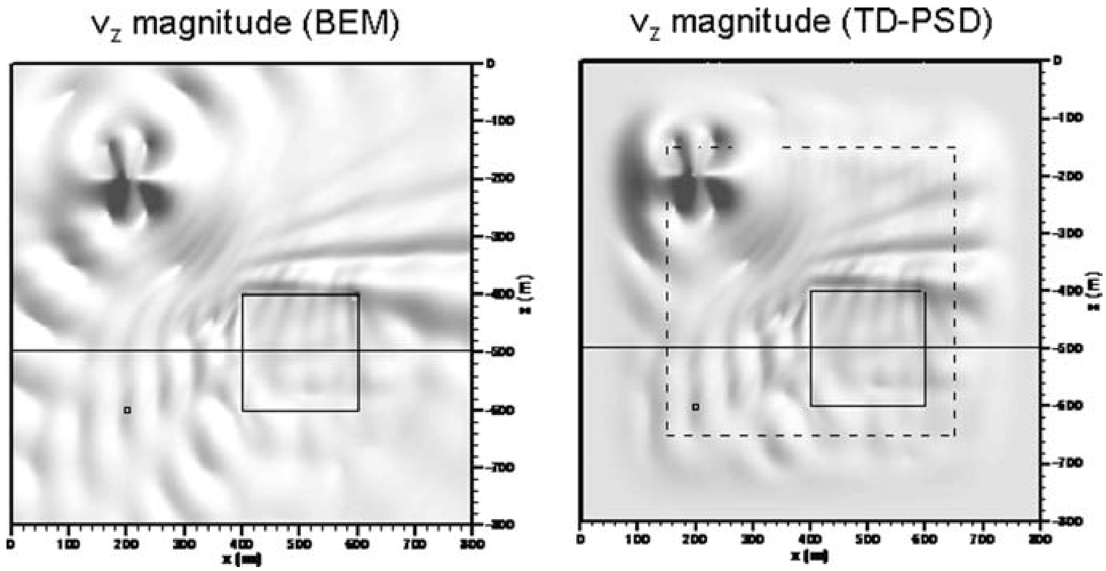

Figure 3. Comparison of the magnitude of the vertical particle velocity computed by: (left) BEM, and (right) TD–PSD. The dashed box in the TD–PSD figure indicates the location of the absorbing boundaries, and the solid box deliniates the high-velocity inclusion. The solid horizontal line is the profile along which the fields are compared in Fig. 4.

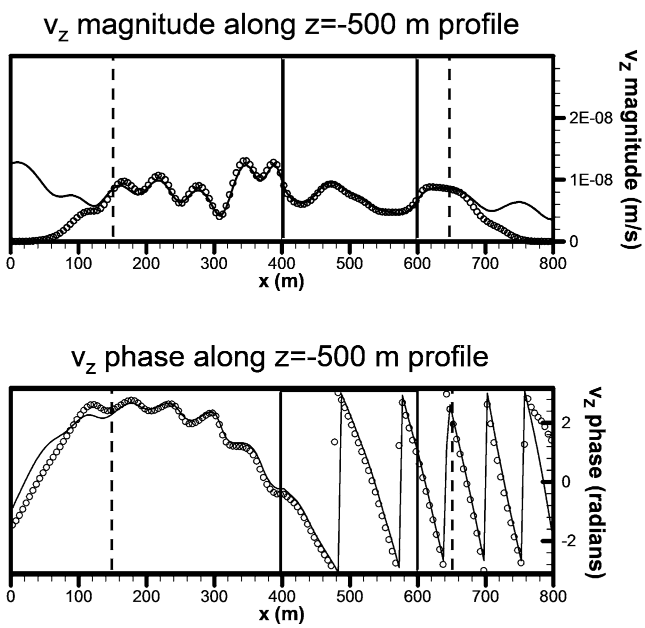

Figure 4. Comparisons of the magnitude and phase of the vertical particle velocity along the profile $z = -500$ m computed by: (solid line) BEM and (circles) TD–PSD. The vertical dashed lines show the location of the absorbing boundaries in the finite difference model, and the vertical solid lines show the location of the high velocity inclusion.

condition required to obtain stable estimates of the magnitudes and phases using PSD. For the case of a source emitting two frequencies, the following analysis will show that stable estimates of the magnitude and phase can be obtained by integrating over the inverse of a beating frequency defined by the difference of the two frequencies.

To demonstrate this, consider the case of two cosine waves with different frequencies ω_1 and ω_2 being injected into a medium (either two separate sources, or a single source emitting the superposition of two cosine waves),

$$\begin{aligned}
\varepsilon_{\text{sig}} &= E_{\text{sig1}} \cos(\omega_1 t + \theta_{\text{sig1}}) + E_{\text{sig2}} \cos(\omega_2 t + \theta_{\text{sig2}}) \quad \text{signal} \\
\varepsilon_{\text{ref1}(0^\circ)} &= E_{\text{ref1}} \cos(\omega_1 t + \theta_{\text{ref1}}) \text{ reference (in-phase } \omega_1) \\
\varepsilon_{\text{ref1}(90^\circ)} &= E_{\text{ref1}} \cos(\omega_1 t + \theta_{\text{ref1}} + 90^\circ) \text{ reference (out-of-phase } \omega_1).
\end{aligned} \tag{5}$$

Following eq. (2), form the in-phase component for frequency ω_1 by cross-correlation with the reference,

$$\begin{aligned}
X_1 &= \frac{1}{T_B} \int_0^{T_B} [\varepsilon_{\text{sig}} \cdot \varepsilon_{\text{ref1}(0^\circ)}] dt \\
&= \frac{E_{\text{sig1}} E_{\text{ref1}(0^\circ)}}{2T_B} \int_0^{T_B} \{\cos[\theta_{\text{sig1}} - \theta_{\text{ref1}(0^\circ)}] \\
&\quad + \cos[2\omega_1 t + \theta_{\text{sig1}} + \theta_{\text{ref1}(0^\circ)}]\}\, dt \\
&\quad + \frac{E_{\text{sig2}} E_{\text{ref1}(0^\circ)}}{2T_B} \int_0^{T_B} \{\cos[\Delta\omega_B t + \theta_{\text{sig2}} - \theta_{\text{ref1}(0^\circ)}] \\
&\quad + \cos[(\omega_1 + \Delta\omega_B) t + \theta_{\text{sig2}} - \theta_{\text{ref1}(0^\circ)}]\}\, dt,
\end{aligned} \tag{6}$$

where $\Delta\,\omega_B = (\omega_2 - \omega_1)$, and for simplicity the limits of the integral are relative to the simulation time at which steady-state conditions are achieved (t_s in eqs 2 and 3). If the integration time is selected with the following properties,

$$\begin{aligned}
T_B &= \frac{2\pi}{\Delta\omega_B} \\
\omega_2 &= \omega_1 + n\,\Delta\omega_B, \quad \text{where } n \geq 1 \text{ is an integer},
\end{aligned} \tag{7}$$

then the contribution of signal ω_2 (second integral) drops out, and the in-phase contribution of signal ω_1 is recovered,

$$\begin{aligned}
X_1 &= \frac{\Delta\omega_B\, E_{\text{sig1}} E_{\text{ref1}(0^\circ)}}{4\pi} \int_0^{\frac{2\pi}{\Delta\omega_B}} \{\cos[\theta_{\text{sig1}} - \theta_{\text{ref1}(0^\circ)}] \\
&\quad + \cos[4\pi n\,\Delta\omega_B t + \theta_{\text{sig1}} + \theta_{\text{ref1}(0^\circ)}]\}\, dt \\
&\quad + \frac{\Delta\omega_B\, E_{\text{sig2}} E_{\text{ref1}(0^\circ)}}{4\pi} \int_0^{\frac{2\pi}{\Delta\omega_B}} \{\cos[\Delta\omega_B\, t + \theta_{\text{sig2}} - \theta_{\text{ref1}(0^\circ)}]
\end{aligned}$$

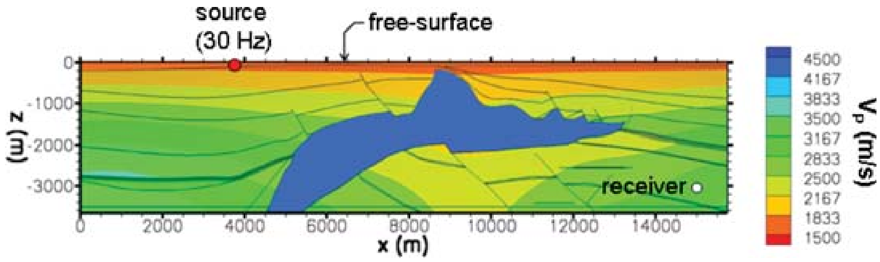

Figure 5. SEG/EAGE salt model used to test the finite difference TD–PSD approach for estimating the frequency response. A 30 Hz source is located near the free-surface, and a monitor receiver is embedded in the bottom-right corner of the model.

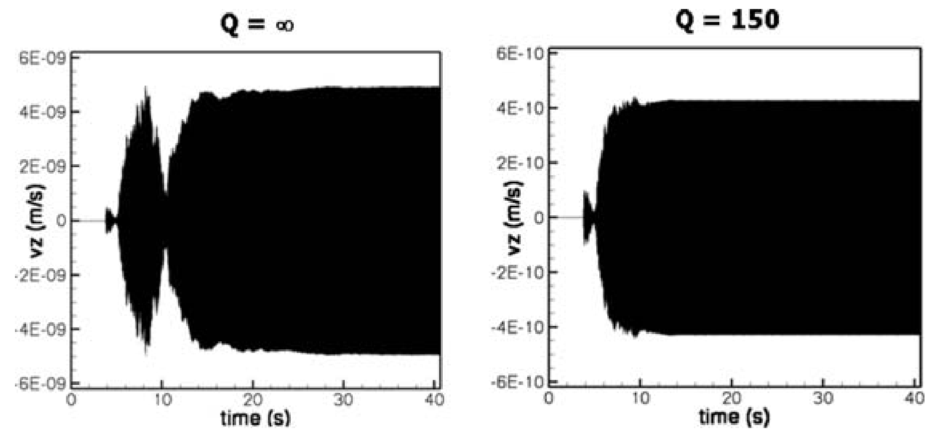

Figure 6. The traces recorded at the monitor receiver (Fig. 5). Note that the effect of adding attenuation to the model ($Q = 150$) is to significantly reduce the time at which steady-state (simple harmonic motion) is achieved.

$$+\cos[(n+1)\Delta\omega_B\, t + \theta_{\mathrm{sig2}} - \theta_{\mathrm{ref1}(0^\circ)}]\}\, dt$$
$$= \frac{E_{\mathrm{sig1}} E_{\mathrm{ref1}(0^\circ)}}{2} \cos[\theta_{\mathrm{sig1}} - \theta_{\mathrm{ref1}(0^\circ)}]. \tag{8}$$

Following the same procedure for the out-of-phase component gives,

$$\begin{aligned} Y_1 &= \frac{1}{T_B}\int_0^{T_B} [\varepsilon_{\mathrm{sig1}} \cdot \varepsilon_{\mathrm{ref1}\,(90^\circ)}]dt \\ &= \frac{\Delta\omega_B\, E_{\mathrm{sig1}} E_{\mathrm{ref1}(90^\circ)}}{4\pi} \int_0^{\frac{2\pi}{\Delta\omega_B}} \{\sin[\theta_{\mathrm{sig1}} - \theta_{\mathrm{ref1}(90^\circ)}] \\ &\quad - \sin[4\pi n \Delta\omega_B t + \theta_{\mathrm{sig1}} + \theta_{\mathrm{ref1}(90^\circ)}]\}\, dt \\ &\quad + \frac{\Delta\omega_B\, E_{\mathrm{sig2}} E_{\mathrm{ref1}(90^\circ)}}{4\pi} \int_0^{\frac{2\pi}{\Delta\omega_B}} \{\sin[\Delta\omega_B\, t + \theta_{\mathrm{sig2}} - \theta_{\mathrm{ref1}(90^\circ)}] \\ &\quad + \sin[(n+1)\Delta\omega_B\, t + \theta_{\mathrm{sig2}} - \theta_{\mathrm{ref1}(90^\circ)}]\}\, dt \\ &= \frac{E_{\mathrm{sig1}} E_{\mathrm{ref1}(90^\circ)}}{2} \sin[\theta_{\mathrm{sig1}} - \theta_{\mathrm{ref1}(90^\circ)}]. \end{aligned} \tag{9}$$

Application of eq. (4) to eqs (8) and (9) gives the estimates of the magnitude and phase for the ω_1 component of the signal. The same analysis can be applied to extract the ω_2 component of the signal. This result demonstrates that recovery of the magnitude and phase for a signal composed of two harmonic waves with different frequencies is possible if the integration time is set to the beating period $T_B = 2\pi/\Delta\,\omega_B$.

This analysis can be generalized to the case of $N_f > 2$ frequencies to show that multifrequency PSD is possible for a signal composed of many frequencies provided that a constant frequency separation $\Delta\omega_B$ is maintained between the frequencies. As with the two frequency example given above, the constant frequency separation for the $N_f > 2$ case allows the PSD integration over $T_B = 2\pi/\Delta\omega_B$ to accurately recover the magnitudes and phases for each frequency component contained in the signal.

3.2 Frequency-encoded sources

Recent work on finite difference FD migration and full-waveform inversion (Mulder & Plessix 2004; Sirgue & Pratt 2004) demonstrate that subsurface imaging of structure and properties is possible with far-fewer frequencies ($N_f < 10$) than prescribed by Nyquist's theorem. This work has also demonstrated that a scale approach to FD inversion in which the inversion is progressed from low frequency to high better ensures convergence to the global solution. Because seismic reflection surveys can have hundreds (2-D) to thousands (3-D) of spatially distributed sources and in order to preserve the scale approach, it is desirable to have a frequency response seismic modelling engine that can efficiently model many sources around a narrow frequency band.

The multifrequency PSD described in Section 3.1 offers the possibility of obtaining the frequency response from many sources in a single finite difference TD simulation by encoding each source with a different frequency. As discussed in the previous section, for more than two frequencies, each frequency should be separated by a constant Δf_B in order for the PSD integration to accurately recover the magnitude and phase.

Fig. 8 shows the layout for three frequency-encoded sources propagating in the SEG/EAGE salt model ($Q = 150$). In this model, the sources have frequencies $f = 30\,\mathrm{Hz} + n\Delta f_B$, where $n = 0, 1, 2$ and $\Delta f_B = 0.1$ Hz. Fig. 9 shows the trace recorded at the receiver located in the bottom right corner of the model (Fig. 8). Comparison of Fig. 9 with the trace from the single source simulation (Fig. 6)

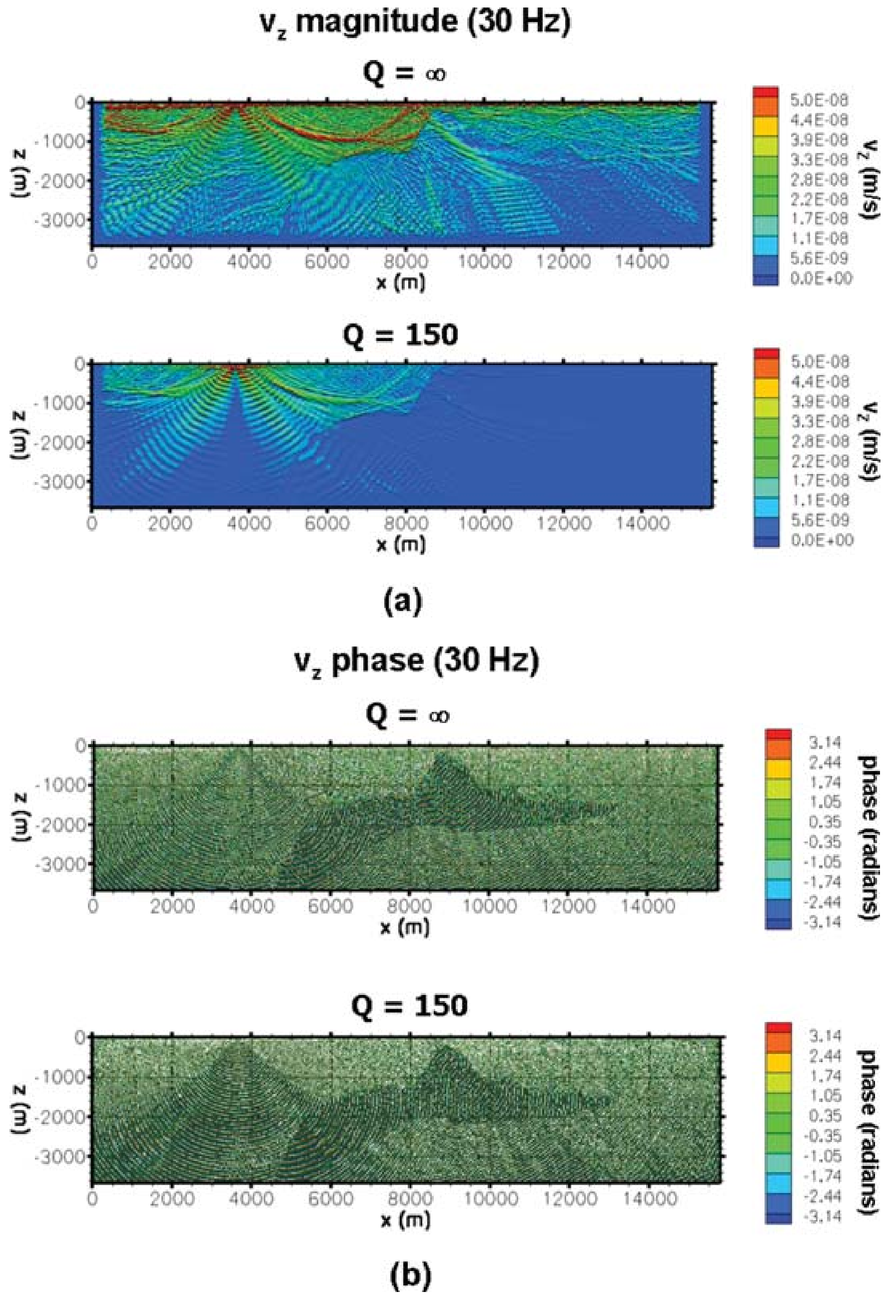

Figure 7. The magnitude (a) and phase (b) fields of the vertical particle velocity computed with finite difference TD–PSD for two Q values.

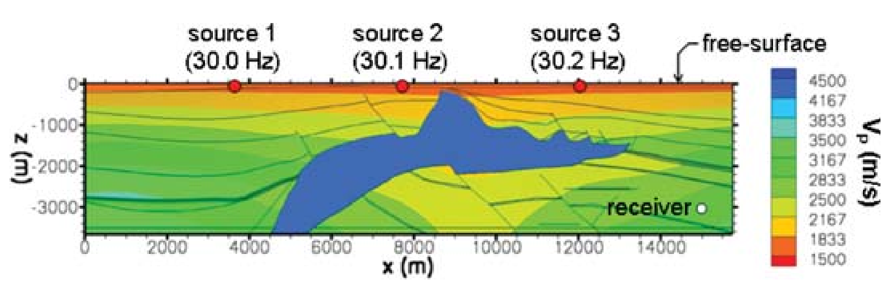

Figure 8. SEG/EAGE salt model with the locations of the three sources used in the multisource test of TD–PSD$_{FES}$. The source frequencies used were 30.0, 30.1 and 30.2 Hz.

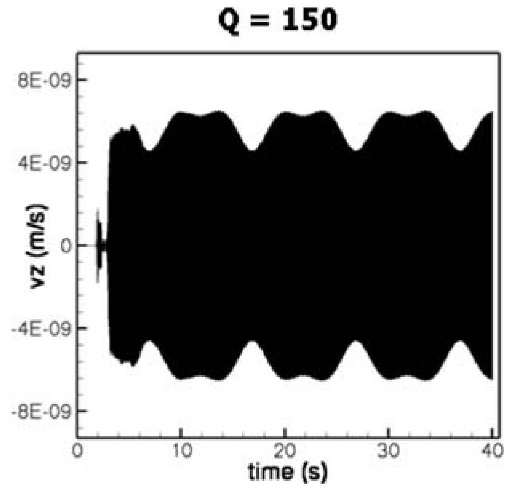

Figure 9. The trace recorded at the monitor receiver for the frequency-encoded three source example (Fig. 8). The frequency difference between each of the three sources, $\Delta f = 0.1$ Hz, gives rise to beating with a period of 10 s.

shows the $T_B = 1/\Delta f_B = 10$ s beating resulting from the superposition of the three frequencies. The magnitude and phase of the vertical particle velocity were computed at every grid location in the finite difference model. These values were then used to reconstruct a snapshot of the time-harmonic wavefield (Fig. 10) using eq. (1). Clear separation of the wavefields for each source can be seen, indicating that the PSD is capable of extracting the wavefield from each source, with negligible contributions from the other sources.

4 ANALYSIS OF THE COMPUTATIONAL REQUIREMENTS FOR 2-D AND 3-D FINITE DIFFERENCE TD–PSD

In this section, we provide estimates of the storage and number of operations (arithmetic complexity) for multisource frequency response modelling using 2-D ($n \times n$) and 3-D ($n \times n \times n$) finite difference TD–PSD. We focus our motivation here on the scale approach to frequency domain full-waveform inversion (discussed at the beginning of Section 3.2) in which the solution strategy is to carry out the inversion for many (spatially distributed) sources, starting at a low frequency and progressing to higher frequencies (Mulder & Plessix 2004; Sirgue & Pratt 2004). For this strategy, the TD–PSD approach can be applied in two flavours: (1) TD–PSD$_{\mathrm{SS}}$ consisting of N_S individual single source runs, with all runs at the same frequency, and (2) TD–PSD$_{\mathrm{FES}}$ consisting of a single run with N_S frequency-encoded sources. In the second approach, the frequency spacing between the frequency encoded sources, Δf_B, is selected such that $N_S \cdot \Delta f_B$ is small (i.e. narrow bandwidth).

The operation count for a 3-D ($n \times n \times n$) finite difference model using the first approach (TD–PSD$_{\mathrm{SS}}$) is

$$\begin{aligned} OC_{(\mathrm{ss})} &= N_S\left[N_t\, n^3\, A + N_T\, n^3 (A + B)\right] \\ &\sim N_S\, N_t\, n^3\, A, \quad \text{for } N_t \gg N_T, \end{aligned} \tag{10}$$

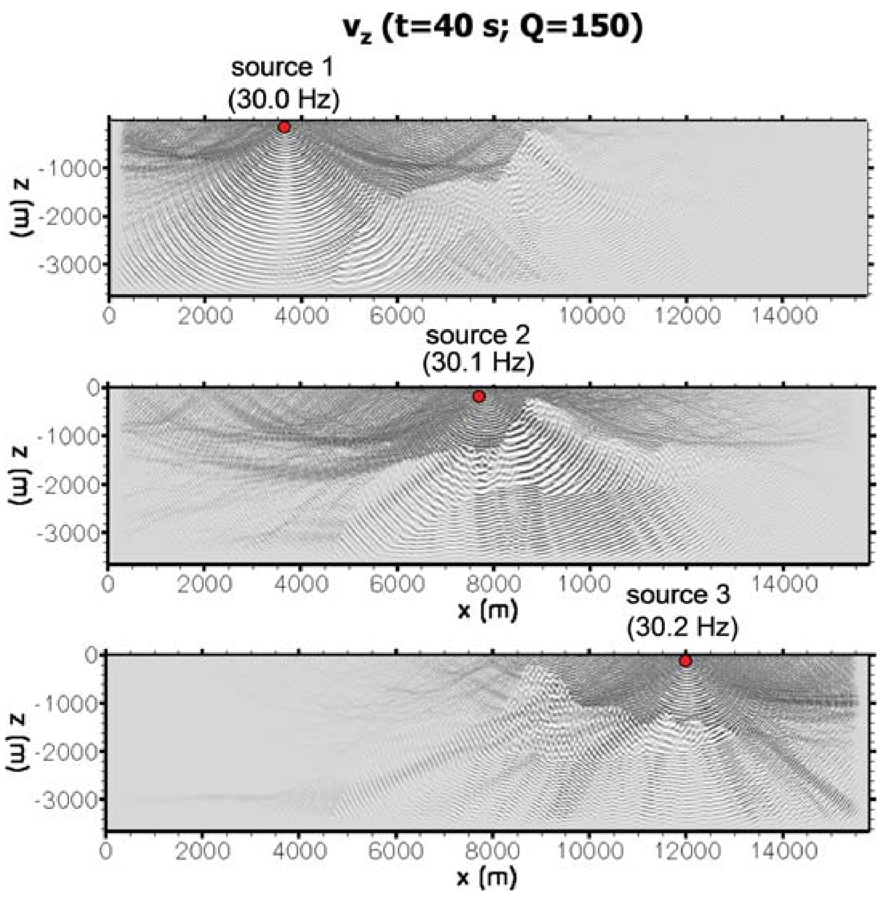

Figure 10. Vertical particle velocity transient fields at 40 s constructed for each of the three sources from the TD–PSD$_{\mathrm{FES}}$ computed magnitudes and phases. The computed wavefields show a clean separation of wave motion coming from each source.

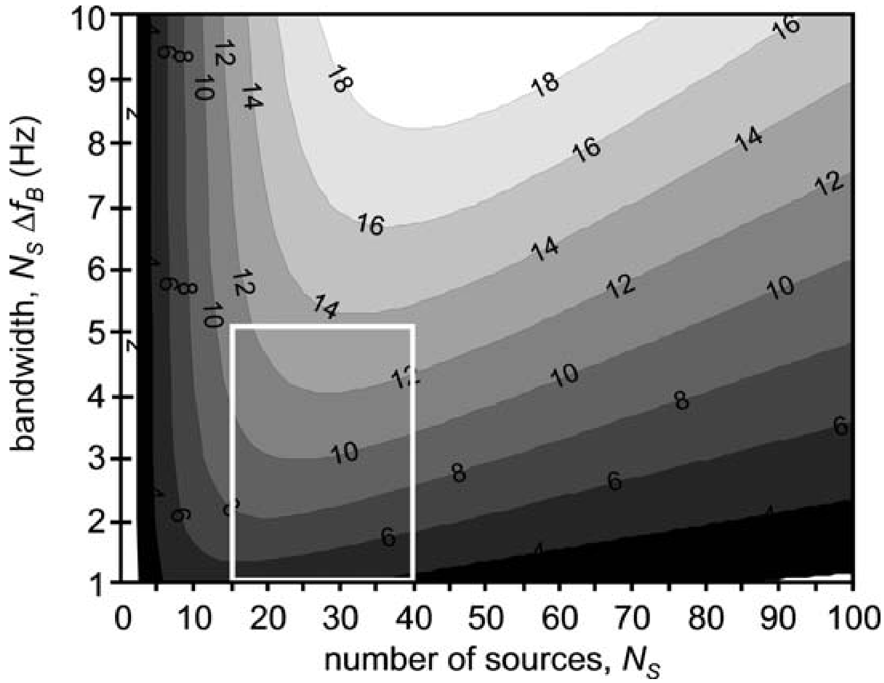

Figure 11. Trade-off plot of the speed-up that can be obtained for multiple source frequency response modelling using frequency encoded sources (TD–PSD$_{\mathrm{FES}}$) relative to the more conventional approach in which each source is modeled in a separate finite difference run (TD–PSD$_{\mathrm{SS}}$). The trade-off is between the number of frequency-encoded sources and the frequency spread (between the first and last source) that can be tolerated. The boxed region highlights the range of speed-ups possible with TD–PSD$_{\mathrm{FES}}$ for 15–40 sources and a frequency bandwidth of 1–5 Hz.

where
$N_S \equiv$ is number of sources
$N_t \equiv$ is number of time steps to reach steady-state
$N_T \equiv$ is number of time samples in one period of the propagating wave
$A \equiv$ is number of operations in the finite difference TD algorithm
$B \equiv$ is number of operations in the PSD algorithm.

The operation count for a 3-D ($n \times n \times n$) finite difference model using the second approach (TD–PSD$_{\mathrm{FES}}$) is

$$\begin{aligned} OC_{(\mathrm{FES})} &= N_t\, n^3\, A + N_{T_B}\, n^3 (A + N_S\, B) \\ &= N_t\, n^3\, A \left\{ 1 + \frac{N_{T_B}}{N_t} \left[1 + N_S \left(\frac{B}{A} \right) \right] \right\}, \end{aligned} \tag{11}$$

where $N_{T_B} = T_B/\Delta t$ is the number of time steps in one beat cycle.

The ratio between eqs (10) and (11) has the form

$$\begin{aligned} R = \frac{OC_{(\mathrm{ss})}}{OC_{(\mathrm{FES})}} &\sim \frac{N_S}{1 + \frac{N_{T_B}}{N_t} \left[1 + N_S \left(\frac{B}{A} \right) \right]} \\ &\sim \frac{N_S}{1 + \frac{1}{\Delta f_B \Delta t\, N_t} \left[1 + N_S \left(\frac{B}{A} \right) \right]}. \end{aligned} \tag{12}$$

When eq. (12) is plotted as a function of the number of sources N_S and the product $N_S \Delta f_B$ (i.e. the frequency bandwidth occupied by the N_S sources each separated by Δf_B), a trade-off curve results Fig. 11). This curve illustrates that if it is desirable to keep the frequency spread between the first and last source in the simulation to a minimum (i.e. a small value of $N_S \Delta f_B$), as in the strategy for FD full-waveform inversion discussed at the beginning of Section 3.2, then there is an optimum number of sources that can be used in TD–PSD$_{\mathrm{FES}}$ to achieve the maximum speed-up over TD–PSD$_{\mathrm{SS}}$. For an assumed ratio of $(B/A) = 1/10$ and an upper bound of $N_S \Delta f_B =$ 5 Hz, the TD–PSD$_{\mathrm{FES}}$ speed-up is $\sim 10\times$ when 15–40 sources are used. Because the model size has dropped out of the ratio eq. (12), this result also holds for 2-D TD–PSD.

Table 1 gives the computational efficiency (big-*O*) estimates for both flavours of TD–PSD for the multiple source problem. Note that these order of magnitude estimates do not reflect the smaller gains described in eq. (12), that is, both flavours of TD–PSD have the same operation counts. Also note that for problems with many sources, TD–PSD$_{\mathrm{FES}}$ requires N_S more storage for the additional magnitude and phase fields for each source.

Also shown in Table 1 for reference are the estimates of storage and number of operations for direct solution of the finite difference FD equations by LU-factorization with the ND re-ordering method (FD–ND; George & Liu 1981). For 2-D problems with many sources, FD–ND is an effective solution strategy: both TD–PSD$_{\mathrm{SS}}$ and TD–PSD$_{\mathrm{FES}}$ require a factor N_S more operations than FD–ND, but TD–PSD$_{\mathrm{SS}}$ has lower storage requirements. For 3-D problems, both TD–PSD approaches have significantly lower number of operations than FD–ND. TD–PSD$_{\mathrm{SS}}$ is superior to both TD–PSD$_{\mathrm{FES}}$ and FD–ND in storage requirements.

The storage and operation count estimates in Table 1 suggest that for most 2-D frequency response modelling problems (many sources, ample memory), FD–ND is the method of choice. For large, memory-limited 3-D problems (e.g. $10\,000 \times 2500 \times 2500$) typical in seismic exploration, multisource frequency response modelling is best addressed with TD–PSD$_{\mathrm{SS}}$, that is, by running N_S single source TD–PSD runs.

5 SUMMARY

This paper presents an approach for computing the frequency response of realistic earth models using an explicit finite difference TD

Table 1. Storage and operation requirements for 2-D ($n \times n$) and 3-D ($n \times n \times n$) multiple source finite difference frequency response modelling: FD–ND denotes frequency domain (FD) solution via nested dissection (ND) re-ordering, and TD–PSD denotes time domain (TD) solution via phase sensitive detection (PSD). N_S is the number of sources, N_t is the number of time steps required to attain a steady-state wavefield (see Appendix A), and N_{T_B} is the number of time steps in one beat period.

Finite difference frequency response modelling	FD–ND	TD–PSD$_{SS}$ (N_S single source runs)	TD–PSD$_{FES}$ (single run with N_S frequency-encoded sources)
2-D Storage	$O(n^2 \log_2 n)$	$O(n^2)$	$O(n^2 N_S)$
2-D #Operations	$O(n^3)$	$O(n^2\ N_t\ N_S) \sim O(n^3\ N_S)$	$O(n^2\ N_{T_B}\ N_S) \sim O(n^3\ N_S)$
3-D Storage	$O(n^4)$	$O(n^3)$	$O(n^3\ N_S)$
3-D #Operations	$O(n^6)$	$O(n^3\ N_t\ N_S) \sim O(n^4\ N_S)$	$O(n^3\ N_{T_B}\ N_S) \sim O(n^4\ N_S)$

code and a PSD algorithm. In the TD–PSD approach, the frequency response of seismic waves is computed by running the finite difference TD code with a harmonic wave source out to steady-state, and then extracting the magnitude and phase from the transient data via a cross-correlation with in-phase and out-of-phase reference cosine waves. The PSD algorithm requires integration over a single cycle of the waveform to obtain accurate phase and magnitude estimates. Because this integration is performed by a running summation overtime, it is not necessary to store waveforms at the grid locations, as would be the case if an FFT was used. Comparisons of the finite difference TD–PSD approach with a FD boundary element method (BEM) solution demonstrate the accuracy of this approach. Simulations in the SEG/EAGE salt model demonstrate the importance of including (realistic) attenuation in the model to reduce the time required to achieve steady-state conditions (simple harmonic motion). It was demonstrated that the TD–PSD approach can be used to obtain the frequency response of multiple sources in a single finite difference TD run by encoding each source with a different frequency (TD–PSD$_{FES}$). The presence of multiple sources gives rise to beating, and analysis of multifrequency PSD demonstrates that the PSD integration must be made over the beat period of the interfering waves to accurately recover the magnitude and phase.

Analysis of the operation counts suggests that significant speedups can be achieved with the frequency-encoded source approach TD–PSD$_{FES}$ relative to the more conventional TD–PSD$_{SS}$ approach where separate single source runs are performed. Analysis of the storage for TD–PSD$_{FES}$, however, indicates that this approach requires significantly more memory to store the magnitude and phase fields for all the sources. For large 3-D problems, this additional storage may render the TD–PSD$_{FES}$ approach intractable. The analysis shows that the straightforward TD–PSD$_{SS}$ approach of running separate finite difference models for each source is the best approach for 3-D frequency response modelling, with significantly lower storage and operations than a direct solution of the finite difference frequency domain equations using nested dissection re-ordering (FD–ND). Further work is required to examine the performance of TD–PSD in realistic 3-D earth models, and to investigate potential avenues for increasing its computation efficiency.

ACKNOWLEDGMENTS

This work was supported by the Director, Office of Science, Office of Basic Energy Sciences, Division of Chemical Sciences, Geosciences, and Biosciences of the US Department of Energy under Contract No. DE-AC03-76SF00098 and by Chevron Energy Technology Company. We thank Jonathan Ajo-Franklin, Valeri Korneev, and Joe Stefani for insightful discussions on monochromatic waves, and the reviewers for improving the content and readability of the paper.

REFERENCES

Aminzadeh, F., Burkhard, N., Nicoletis, L., Rocca, F. & Wyatt, K., 1994. SEG/EAGE 3-D modelling project: 2nd update, *Leading Edge,* **13,** 949–952.

Barrett, R. *et al.*, 1994. *Templates for the Solution of Linear Systems: Building Blocks for Iterative Methods*, SIAM, Philadelphia.

Furse, C.M., 2000. Faster than Fourier-ultra-efficient time-to-frequency domain conversions for FDTD simulations, *Antenn. Propagat. Mag.,* **42,** 24–34.

George, J.A. & Liu, J.W.H., 1981. *Computer Solution of Large Sparse Positive Definite Systems*, Prentice-Hall, New Jersey.

Hustedt, B., Operto, S. & Virieux, J., 2004. Mixed-grid and staggered-grid finite-difference methods for frequency-domain acoustic wave modelling, *Geophys. J. Int.,* **157,** 1269–1296.

Kinsler, L.E., Frey, A.R., Coppens, A.B. & Sanders, J.V., 1982. *Fundamentals of Acoustics*, 3rd edn, John Wiley & Sons, New York, pp. 20–23.

Levander, A.R., 1988. Fourth-order finite-difference *P-SV* seismograms, *Geophysics,* **53,** 1425–1436.

Li, X.S. & Demmel, J., 2003. SuperLU_DIST: A scalable distributed-memory sparse direct solver for unsymmetric linear systems, *ACM Trans. Math. Software,* **29,** 110–140. http://crd.lbl.gov/~xiaoye/SuperLU/

Marfurt, K.J., 1984, Accuracy of finite difference and finite element modelling of the scalar and elastic wave equations, *Geophysics,* **49,** 533–549.

Mulder, W.A. & Plessix, R.-E., 2004. How to choose a subset of frequencies in frequency-domain finite-difference migration, *Geophys. J. Int.,* **158,** 801–812.

Nihei, K.T., 2005. *BE2D: A 2D Boundary Element Code for Computing the Frequency Response of Elastic Waves in Heterogeneous Media with Imperfect Interfaces*, Lawrence Berkeley National Laboratory Report, **LBNL-58685,** Berkeley.

Plessix, R.E. & Mulder, W.A., 2003. Separation-of-variables as a preconditioner for an iterative Helmholtz solver, *Appl. Numer. Math.,* **44,** 385–400.

Pratt, R.G., Shin, C. & Hicks, G.J., 1998. Gauss-Newton and full Newton methods in frequency space seismic waveform inversion, *Geophys. J. Int.,* **133,** 341–362.

Press, W.H., Teukolsky, S.A., Vetterling, W.T. & Flannery, B.P., 1992. *Numerical Recipes in C*, 2nd edn, Cambridge University Press, Cambridge, p. 504.

Robertsson, J.O.A., Blanch, J.O. & Symes, W.W., 1994. Viscoelastic finite-difference modelling, *Geophysics,* **59,** 1444–1456.

Sirgue, L. & Pratt, R.G., 2004. Efficient waveform inversion and imaging: A strategy for selecting temporal frequencies, *Geophysics,* **69,** 231–248.

Stanford Research Systems, 1999. DSP Lock-In Amplifier Model 850, Rev. 1.4. http://www.thinksrs.com/downloads/PDFs/Manuals/SR830m.pdf

Štekl, I. & Pratt, R.G., 1998. Accurate viscoelastic modelling by frequency-domain finite differences using rotated operators, *Geophysics,* **63,** 1779–1794.

APPENDIX A: DEMONSTRATION THAT $N_t \sim O(n)$

Let the number of time steps that a 2-D ($n \times n$) or 3-D ($n \times n \times n$) finite difference TD code must be run to in order to attain steady-state wavefields (i.e. simple harmonic motion) be defined as

$$N_t = \frac{t_S}{\Delta t}. \tag{A1}$$

In eq. (A1), t_S is selected large enough to include the slowest arrivals coming from the most distant parts of the model. As a conservative estimate, we take this to be the traveltime it takes a shear wave to propagate across five lengths $5L$ of the largest model dimension at the slowest shear velocity $V_{S\min}$ contained in the model

$$t_S = \frac{5L}{V_{S\min}} = \frac{5\,n\,\Delta l}{V_{S\min}}, \tag{A2}$$

where Δl is the grid size. We will see at the end of this analysis that doubling or tripling this distance estimate will not alter the final result. The time step Δt is prescribed by the stability condition for a fourth order spatial differencing scheme (Levander 1988)

$$\Delta t \leq \frac{\Delta l}{\sqrt{2}\, V_{P\max} \sum_{i=0,1} |c_i|} = 0.6061\ \Delta l / V_{P\max}, \tag{A3}$$

where $c_0 = 9/8$ and $c_1 = -1/24$ are the inner and outer coefficients of the fourth order approximation to the first derivative.

Substituting eqs (A2) and (A3) into eq. (A1) gives

$$N_t = \frac{5\,n}{0.6061\,(V_{S\min}/V_{P\max})} \sim O(n). \tag{A4}$$

Because ‘ big-O ’ notation operation estimates are essentially proportionality estimates for large inputs (i.e. large n), it is clear that the relation (A4) still holds even if we had used a larger estimate of the maximum propagation path.